crystals

MDPI

Article

Microwave-Employed Sol–Gel Synthesis of Scheelite-Type Microcrystalline $AgGd(MoO_4)_2$:Yb^{3+}/Ho^{3+} Upconversion Yellow Phosphors and Their Spectroscopic Properties

Chang Sung Lim [1,*], Aleksandr Aleksandrovsky [2,3], Victor Atuchin [4,5,6,*], Maxim Molokeev [7,8,9] and Aleksandr Oreshonkov [10,11]

1 Department of Aerospace Advanced Materials Engineering, Hanseo University, Seosan 31962, Korea
2 Laboratory of Coherent Optics, Kirensky Institute of Physics Federal Research Center KSC SB RAS, 660036 Krasnoyarsk, Russia; aleksandrovsky@kirensky.ru
3 Institute of Nanotechnology, Spectroscopy and Quantum Chemistry, Siberian Federal University, 660041 Krasnoyarsk, Russia
4 Laboratory of Optical Materials and Structures, Institute of Semiconductor Physics, SB RAS, 630090 Novosibirsk, Russia
5 Laboratory of Semiconductor and Dielectric Materials, Novosibirsk State University, 630090 Novosibirsk, Russia
6 Research and Development Department, Kemerovo State University, 650000 Kemerovo, Russia
7 Laboratory of Crystal Physics, Kirensky Institute of Physics, Federal Research Center KSC SB RAS, 660036 Krasnoyarsk, Russia; msmolokeev@mail.ru
8 Institute of Engineering Physics and Radioelectronics, Siberian Federal University, 660041 Krasnoyarsk, Russia
9 Department of Physics, Far Eastern State Transport University, 680021 Khabarovsk, Russia
10 Laboratory of Molecular Spectroscopy, Kirensky Institute of Physics Federal Research Center KSC SB RAS, 660036 Krasnoyarsk, Russia; oreshonkov@iph.krasn.ru
11 School of Engineering and Construction, Siberian Federal University, 660041 Krasnoyarsk, Russia
* Correspondence: cslim@hanseo.ac.kr (C.S.L.); atuchin@isp.nsc.ru (V.A.)

Received: 12 October 2020; Accepted: 29 October 2020; Published: 4 November 2020

Abstract: $AgGd(MoO_4)_2$:Ho^{3+}/Yb^{3+} double molybdates with five concentrations of Ho^{3+} and Yb^{3+} were synthesized by the microwave employed sol–gel based process (MES), and the crystal structure variation, concentration effects, and spectroscopic characteristics were investigated. The crystal structures of $AgGd_{1-x-y}Ho_xYb_y(MoO_4)_2$ (x = 0, 0.05; y = 0, 0.35, 0.4, 0.45, 0.5)at room temperature were determined in space group $I4_1/a$ by Rietveld analysis. Pure $AgGd(MoO_4)_2$ has a scheelite-type structure with mixed occupations of (Ag,Gd) sites and cell parameters a = 5.24782 (11) and c = 11.5107 (3) Å, V = 317.002 (17) Å^3, Z = 4. In doped samples, the sites are occupied by a mixture of (Ag,Gd,Ho,Yb) ions, which provides a linear cell volume decrease with the doping level increase. Under the excitation at 980 nm, AGM:0.05Ho,yYb phosphors exhibited a yellowish green emission composed of red and green emission bands according to the strong transitions $^5F_5 \rightarrow {}^5I_8$ and $^5S_2/{}^5F_4 \rightarrow {}^5I_8$ of Ho^{3+} ions. The evaluated photoluminescence and Raman spectroscopic results were discussed in detail. The upconversion intensity behavior dependent on the Yb/Ho ratio is explained in terms of the optimal number of Yb^{3+} ions at the characteristic energy transfer distance around the Ho^{3+} ion.

Keywords: microwave sol–gel; double molybdate; yellow phosphors; upconversion; spectroscopic properties

1. Introduction

In the last years, rare earth (RE) doped light emitters, based on the frequency upconversion (UC), have been extensively investigated and applied in fields such as optoelectronics as solid state laser devices, display technology, light emitting diode (LED) materials, solar energy cell compositions, and biological imaging sensors [1–4]. In UC phosphors, the conversion of near infrared photons to visible photons is reached via a multiphoton absorption process, and finely crystallized host materials are needed to decrease energy losses in multistage electronic transitions. Among such crystals, RE-containing molybdates are widely investigated in terms of searching for new structures, including structure-modulation effects, promising spectroscopic characteristics, and excellent UC photoluminescence (PL) properties [5–12]. In this aspect, binary RE-containing tetragonal molybdates of general composition $ARE(MoO_4)_2$ (A = Li, Na, K. Ag) and scheelite-type (ST) structure are of particular interest. The ST compounds crystallize in tetragonal space group $I4_1/a$ and this crystal family is characterized by wide possibility for the substitution of RE activators at RE sites without structure disruption and significant defect generation. The complex ST molybdates are extensively investigated as host materials in the phosphor preparation and laser technology, respectively [13–24].

The present study is aimed at the synthesis and evaluation of $AgGd(MoO_4)_2$:Yb^{3+},Ho^{3+} phosphor materials. This molybdate is selected as a representative member of the $AgRE(MoO_4)_2$ group. Generally, ST molybdates $AgRE(MoO_4)_2$ are less studied and, as for $AgGd(MoO_4)_2$, only the space group and cell parameters were determined in the past [25] and such basic properties as its crystal structure and spectroscopic characteristics remain unknown. However, there are two reports on the application of $AgGd(MoO_4)_2$ as a host in phosphor materials [26,27]. In modern UC materials, operable under the excitation at 980 nm of compact high-power laser diodes, such trivalent RE ions as Ho^{3+}, Tm^{3+}, and Er^{3+} are commonly used as activators and, in most cases, Yb^{3+} is applied as a sensitizer. During the UC process, the Ho^{3+} ion can efficiently convert infrared light to a visible spectral range owing to an appropriate energy level configuration. As a sensitizer, the Yb^{3+} ion can be smoothly excited by a proper incident light source working at ~980 nm because this ion has a high absorption cross section at this wavelength. Thus, the co-doped Ho^{3+} and Yb^{3+} ions can be usefully employed pairwise and drastically enhance the UC efficiency via the consequent energy transfer (ET) process from Yb^{3+} to Ho^{3+} [28].

Regarding the methods developed for the synthesis of oxide phosphor compounds, the microwave employed sol–gel (MES) technique has the advantages of a very short process time, stable and homogenous particles, particle size range suitable for the UC process, and high purity resultant products [29–34]. It was found that the MES process can provide efficient results accompanying the highly homogeneous morphology and very stable structures. In the present study, the $AgGd(MoO_4)_2$:Ho^{3+},Yb^{3+} double molybdates with various concentration ratios Yb^{3+}/Ho^{3+} = 7, 8, 9, 10 were synthesized by the MES-based process, and the crystal structure, composition effects, and spectroscopic characteristics were investigated. Scanning electron microscopy (SEM) was employed to evaluate the crystalline morphology. By the UC measurements using excitation at 980 nm, the resultant phosphors were evaluated and strong $^5S_2/^5F_4 \rightarrow {}^5I_8$ transitions (in the green spectral range) and intense transitions of $^5F_5 \rightarrow {}^5I_8$ (in the red spectral range) of Ho^{3+} were observed in terms of the ET process. The evaluated UC, Commission Internationale de L'Eclairage (CIE) coordinates, and Raman spectroscopic results were discussed in detail.

2. Experimental Procedure

In the present experiment, the fabrication of AGM:xHo,yYb ($AgGd_{1-x-y}Ho_xYb_y(MoO_4)_2$) double molybdates with the precise doping of *x*Ho,*y*Yb (x = 0, 0.05; y = 0, 0.35, 0.4, 0.45, 0.5) was carried out by the MES process. In the preparation of AGM:HoYb materials, $AgNO_3$ at purity 99.9% were received from Kojima Chemicals, Japan, $(NH_4)_6Mo_7O_{24}{\cdot}4H_2O$ at purity of 99.0%, as well as $Gd(NO_3)_3{\cdot}6H_2O$, $Yb(NO_3)_3{\cdot}5H_2O$ and $Ho(NO_3)_3{\cdot}5H_2O$ at of purity 99.9%, were used as received from Sigma-Aldrich, USA. Besides, citric acid (CA) at purity 99.5% was received from Daejung Chemicals,

Korea. Distilled water (DW), ethylene glycol (EG, A.R.), and NH_4OH (A.R.) were used to bring about the transparent sol formation.

As the first sequence, to prepare the sol state of (a) $AgGd(MoO_4)_2$ (AGM), $(NH_4)_6Mo_7O_{24}{\cdot}4H_2O$ for 0.057 mol% was slowly dissolved in 80 mL of NH_4OH (8M) with 20 mL of EG under a slight heat-treatment. Simultaneously, $AgNO_3$ for 0.4 mol% and $Gd(NO_3)_3{\cdot}5H_2O$ for 0.4 mol% were carefully weighed and dissolved very slowly in 100 mL of DW under a slight heat treatment. Then, these two solutions were combined under a vigorous stirring. The CA molar ratio accounting to the numbers of all cation metal (CM) ions should be adjusted to 2:1 (CA/CM). The total volume of the combined solution, 180–200 mL, was heat-treated at ~80–100 °C in Pyrex glass (450 mL) before the MES processing. Finally, the consequent solution reveals a highly transparent state.

As for the doped compounds of AGM:xHo,yYb, the following variations were made for which to prepare the solutions: (b) AGM:0.05Ho,0.35Yb, $Gd(NO_3)_3{\cdot}6H_2O$ for 0.24 mol%, $Yb(NO_3)_3{\cdot}5H_2O$ for 0.14 mol%, and $Ho(NO_3)_3{\cdot}5H_2O$ for 0.02 mol%; (c) AGM:0.05Ho, 0.4Yb, $Gd(NO_3)_3{\cdot}6H_2O$ for 0.22 mol%, $Yb(NO_3)_3{\cdot}5H_2O$ for 0.16 mol%, and $Ho(NO_3)_3{\cdot}5H_2O$ for 0.02 mol%; (d) AGM:0.05Ho, 0.45Yb, $Gd(NO_3)_3{\cdot}6H_2O$ for 0.2 mol%, $Yb(NO_3)_3{\cdot}5H_2O$ for 0.18 mol%, and $Ho(NO_3)_3{\cdot}5H_2O$ for 0.02 mol%; and (e) AGM:0.05Ho,0.5Yb, $Gd(NO_3)_3{\cdot}6H_2O$ for 0.18 mol%, $Yb(NO_3)_3{\cdot}5H_2O$ for 0.2 mol%, and $Ho(NO_3)_3{\cdot}5H_2O$ for 0.02 mol%. The MES-derived process algorithm was previously reported and can be found elsewhere [7,10,12].

The structural properties of synthesized samples were evaluated by XRD analysis. The powder XRD patterns of the AGM:xHo,yYb particles for Rietveld analysis were precisely recorded over the angle range of $2\theta = 5–90°$ at room temperature with a D/MAX 2200 (Rigaku in Japan) diffractometer with the use of Cu-Kα radiation and $\theta-2\theta$ geometry. The 2θ size step was 0.02°, and the counting time was 5 s per step. The TOPAS 4.2 package was applied for the Rietveld analysis [35]. The typical microstructure and surface morphology of the obtained particles were observed using SEM (JSM−5600, JEOL in Japan) methods. The PL spectra were relatively recorded at room temperature using a spectrophotometer (Perkin Elmer LS55 in UK). The Raman spectra measurements were performed using an LabRam Aramis (Horiba Jobin-Yvon in France) with the spectral resolution of 2 cm^{-1}. The 514.5 nm line of an Ar ion laser was used as an excitation source and, to avoid the sample decomposition, the power on the samples was kept at the 0.5 mW level.

3. Results and Discussion

The difference Rietveld plots of AGM and AGM:xHo,yYb samples are shown in Figure 1. All diffraction peaks are obviously indexed by the tetragonal cell ($I4_1/a$) with cell parameters close to those of $AgEu(MoO_4)_2$ [36] and $NaGd(MoO_4)_2$ [37]. Therefore, these crystal structures were taken as a starting model in Rietveld refinement. The site of (Ag/Eu) or (Na/Gd) ions was considered as that occupied by Ag, Gd, Ho, and Yb ions with fixed occupations according to the suggested formulas, because no loss channel of starting chemicals is expected in the synthesis. The refinement was stable and gave low R-factors (Figure 1). The main parameters of processing and refinement of the AGM and AGM:xHo,yYb samples are presented in Table 1. The crystal structure of AGM:xHo,yYb is shown in Figure 2. The fractional atom coordinates and isotropic displacement parameters ($Å^2$) of the samples are given in Table 2. The main bond lengths (Å) in AGM and AGM:xHo,yYb structures are presented in Table 3. As seen in Figure 1f, the linear decrease of unit cell volume per decrease of average ion radii IR(Ag/Gd/Ho/Yb) on doping is observed in the AGM and AGM:xHo,yYb molybdates, which proves the suggested chemical formula $AgGd_{1-x-y}Ho_xYb_y(MoO_4)_2$ of the solid solution. The obtained crystallographic data are deposited in Cambridge Crystallographic Data Centre (CSD # 2035192−2035196). The data can be downloaded from the site (www.ccdc.cam.ac.uk/data_request/cif).

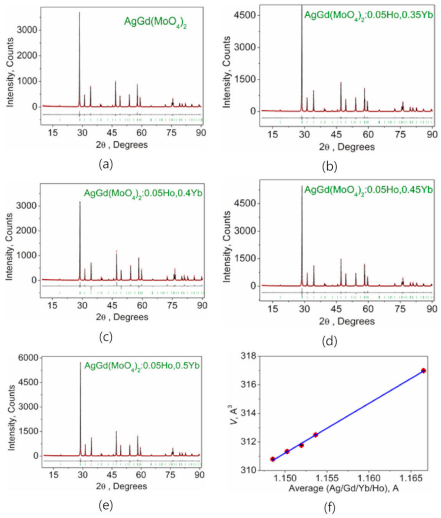

Figure 1. Difference Rietveld plots of $AgGd_{1-x-y}Ho_xYb_y(MoO_4)_2$: (**a**) x = 0, y = 0; (**b**) x = 0.05, y = 0.35; (**c**) x = 0.05, y = 0.4; (**d**) x = 0.05, y = 0.45; (**e**) x = 0.05, y = 0.5. (**f**) Cell volume per average ion radii IR(Ag/Gd/Ho/Yb) in $AgGd_{1-x-y}Ho_xYb_y(MoO_4)_2$.

Table 1. Main parameters of processing and refinement of the $AgGd_{1-x-y}Ho_xYb_y(MoO_4)_2$ samples.

Compound	$AgGd(MoO_4)_2$	$AgGd_{0.6}Ho_{0.05}Yb_{0.35}(MoO_4)_2$	$AgGd_{0.55}Ho_{0.05}Yb_{0.4}(MoO_4)_2$	$AgGd_{0.5}Ho_{0.05}Yb_{0.45}(MoO_4)_2$	$AgGd_{0.45}Ho_{0.05}Yb_{0.5}(MoO_4)_2$
x	0	0.05	0.05	0.05	0.05
y	0	0.35	0.4	0.45	0.5
Sp.Gr.	$I4_1/a$	$I4_1/a$	$I4_1/a$	$I4_1/a$	$I4_1/a$
a, Å	5.24782 (11)	5.22237 (8)	5.21802 (13)	5.21598 (9)	5.21239 (8)
c, Å	11.5107 (3)	11.4581 (2)	11.4498 (3)	11.4455 (2)	11,4394 (3)
V, Å^3	317.002 (17)	312.497 (11)	311.753 (18)	311.392 (12)	310,798 (12)
Z	4	4	4	4	4
2θ-interval, °	5–90	5–90	5–90	5–90	5–90
R_{wp}, %	19.23	16.50	21.86	16.64	16.06
R_p, %	11.91	9.71	15.08	10.55	9.61
R_{exp}, %	16.76	14.91	17.00	14.33	13.87
R_B, %	3.14	1.93	8.65	2.50	2.31
χ^2	1.15	1.11	1.29	1.16	1.16

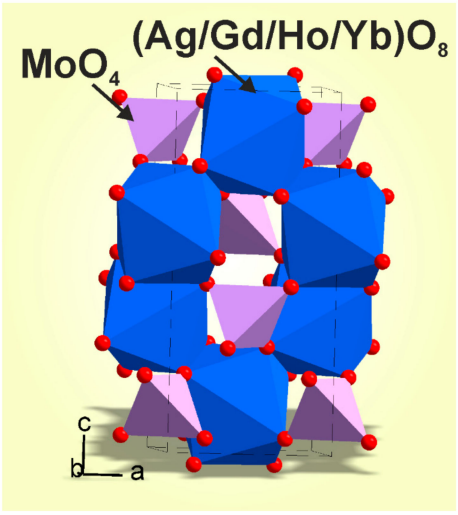

Figure 2. Crystal structure of $AgGd_{1-x-y}Ho_xYb_y(MoO_4)_2$. The unit cell is outlined. The lone atoms are omitted for clarity.

Table 2. Fractional atomic coordinates and isotropic displacement parameters (Å^2) of $AgGd_{1-x-y}Ho_xYb_y(MoO_4)_2$ samples.

	x	*y*	*z*	B_{iso}	Occ.
			$AgGd(MoO_4)_2$		
Ag	0	0.25	0.625	0.6 (3)	0.5
Gd	0	0.25	0.625	0.6 (3)	0.5
Mo	0	0.25	0.125	0.5 (3)	1
O	0.242 (3)	0.1068 (17)	0.0408 (8)	0.8 (4)	1
			$AgGd_{0.6}Ho_{0.05}Yb_{0.35}(MoO_4)_2$		
Ag	0	0.25	0.625	0.3 (3)	0.5
Gd	0	0.25	0.625	0.3 (3)	0.3
Ho	0	0.25	0.625	0.3 (3)	0.025
Yb	0	0.25	0.625	0.3 (3)	0.175
Mo	0	0.25	0.125	0.5 (3)	1
O	0.237 (2)	0.1015 (15)	0.0394 (7)	0.8 (4)	1
			$AgGd_{0.55}Ho_{0.05}Yb_{0.4}(MoO_4)_2$		
Ag	0	0.25	0.625	0.2 (3)	0.5
Gd	0	0.25	0.625	0.2 (3)	0.275
Ho	0	0.25	0.625	0.2 (3)	0.025
Yb	0	0.25	0.625	0.2 (3)	0.2
Mo	0	0.25	0.125	0.5 (3)	1
O	0.240 (3)	0.1043 (19)	0.0412 (9)	0.5 (4)	1
			$AgGd_{0.5}Ho_{0.05}Yb_{0.45}(MoO_4)_2$		
Ag	0	0.25	0.625	0.5 (3)	0.5
Gd	0	0.25	0.625	0.5 (3)	0.25
Ho	0	0.25	0.625	0.5 (3)	0.025
Yb	0	0.25	0.625	0.5 (3)	0.225
Mo	0	0.25	0.125	0.8 (2)	1
O	0.238 (3)	0.1010 (15)	0.0393 (7)	1.1 (4)	1
			$AgGd_{0.45}Ho_{0.05}Yb_{0.5}(MoO_4)_2$		
Ag	0	0.25	0.625	0.5 (3)	0.5
Gd	0	0.25	0.625	0.5 (3)	0.225
Ho	0	0.25	0.625	0.5 (3)	0.025
Yb	0	0.25	0.625	0.5 (3)	0.25
Mo	0	0.25	0.125	0.6 (3)	1
O	0.239 (2)	0.1041 (14)	0.0393 (6)	0.6 (4)	1

It is interesting to consider the field of structural parameters available for $ARE(MoO_4)_2$ (A = Li, Na, K. Ag) compounds of the ST structure. All of the $ARE(MoO_4)_2$ compounds, the unit cell parameters of which are presently known, are listed in Table 4 and shown in Figure 3. As is evident from Table 4, the giant cell volume variation, by ~25%, is possible in the $ARE(MoO_4)_2$ crystal family, which indicates the high stability of this structure.

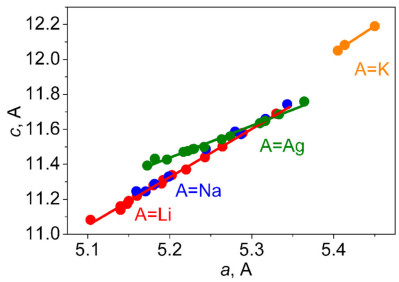

Figure 3. Cell parameter field c–a of $AB(MoO_4)_2$ (A = Li, Na, Ag, K; B = RE) crystallized in space group $I4_1/a$.

Table 3. Main bond lengths (Å) of $AgGd_{1-x-y}Ho_xYb_y(MoO_4)_2$ samples.

$AgGd(MoO_4)_2$			
(Ag/Gd)—O^i	2.458 (12)	Mo—O	1.765 (13)
(Ag/Gd)—O^{ii}	2.506 (12)		
$AgGd_{0.6}Ho_{0.05}Yb_{0.35}(MoO_4)_2$			
(Ag/Gd/Ho/Yb)—O^i	2.494 (9)	Mo—O	1.759 (9)
(Ag/Gd/Ho/Yb)—O^{ii}	2.457 (9)		
$AgGd_{0.55}Ho_{0.05}Yb_{0.4}(MoO_4)_2$			
(Ag/Gd/Ho/Yb)—O^i	2.486 (13)	Mo—O	1.751 (13)
(Ag/Gd/Ho/Yb)—O^{ii}	2.458 (12)		
$AgGd_{0.5}Ho_{0.05}Yb_{0.45}(MoO_4)_2$			
(Ag/Gd/Ho/Yb)—O^i	2.486 (13)	Mo—O	1.763 (12)
(Ag/Gd/Ho/Yb)—O^{ii}	2.451 (11)		
$AgGd_{0.45}Ho_{0.05}Yb_{0.5}(MoO_4)_2$			
(Ag/Gd/Ho/Yb)—O^i	2.494 (9)	Mo—O	1.758 (9)
(Ag/Gd/Ho/Yb)—O^{ii}	2.442 (8)		

Symmetry codes: **(i)** $-x + 1/2, -y, z + 1/2$; **(ii)** $y-1/4, -x + 3/4, z + 3/4$.

Table 4. Cell parameters of $AB(MoO_4)_2$ compounds with $I4_1/a$ space group.

A	B	*a*, Å	*c*, Å	*V*, Å^3	References
Li	Lu	5.10332	11.0829	288.6417	[36]
Li	Yb	5.14	11.14	294.31	[38]
Li	Tm	5.14	11.16	294.84	[38]
Li	Y	5.148	11.173	296.106	[39]
Li	Er	5.15	11.19	296.79	[38]
Li	Ho	5.16	11.22	298.74	[38]
Li	Dy	5.18	11.28	302.67	[38]
Li	Tb	5.19	11.29	304.11	[38]
Li	Gd	5.192	11.31	304.88	[40]
Li	Eu	5.202625	11.33824	306.896	[36]
Li	Sm	5.22	11.37	309.81	[40]
Li	Nd	5.243	11.44	314.47	[39]
Li	Pr	5.2643	11.5011	318.728	[41]
Li	Ce	5.289	11.58	323.93	[42]
Li	La	5.33	11.69	332.10	[38]
Na	Lu	5.1593	11.246	299.350	[21]
Na	Yb	5.170642	11.2454	300.652	[43]
Na	Er	5.1816	11.288	303.07	[44]
Na	Y	5.1989	11.3299	306.231	[45]
Na	Gd	5.244	11.487	315.887	[37]
Na	Eu	5.2797	11.5869	322.988	[46]
Na	Nd	5.2871	11.5729	323.502	[47]
Na	Ce	5.3167	11.66	329.597	[48]
Na	La	5.3433	11.7432	335.278	[49]
K	Pr	5.405	12.05	352.03	[50]
K	Ce	5.4134	12.0821	354.065	[51]
K	La	5.45	12.19	362.07	[49]
Ag	Lu	5.172556	11.39257	304.812	[36]
Ag	Yb	5.1819	11.4317	306.965	[52]
Ag	Tm	5.1966	11.4271	308.585	[52]
Ag	Ho	5.2168	11.471	312.183	[52]
Ag	$Gd_{0.9}Eu_{0.1}$	5.222	11.476	312.94	[27]
Ag	Gd	5.2282	11.4869	313.984	[25]
Ag	Dy	5.2296	11.4883	314.190	[53]
Ag	Tb	5.242	11.4995	315.990	[52]
Ag	Eu	5.26334	11.54333	319.782	[36]
Ag	Sm	5.2739	11.56	321.53	[54]
Ag	Nd	5.3099	11.6352	328.055	[54]
Ag	Pr	5.3164	11.648	329.220	[54]
Ag	Ce	5.3333	11.686	332.398	[54]
Ag	La	5.364	11.7588	338.330	[54]

As seen in Figure 3, on the a–c plane, the $ARE(MoO_4)_2$ (A = Li, Na) crystals lie on the straight line determined by the relation c = 2.76(5) × a − 3.0(2)Å. Three known $KRE(MoO_4)_2$ compounds also determine the straight line nearly parallel to that of $ARE(MoO_4)_2$ (A = Li, Na) molybdates and this line is determined by the relation c = 3.1(1) × a − 4.5(7)Å. In $KRe(MoO_4)_2$ compounds, the boundary of the existence of the ST structure is reached and $KNd(MoO_4)_2$ crystallizes in monoclinic space group $P2_1/n$ [55]. It is unexpected, but the $AgRE(MoO_4)_2$ crystals lie on the new straight line with a more shallow slope and the equation c = 1.9(3) × a + 1.83(6)Å. Thus, the structural behavior of $AgRE(MoO_4)_2$ with the ST structure is specific and is different from that of $ARE(MoO_4)_2$ (A = Li, Na, K) compounds. As for the position of $AgGd(MoO_4)_2$, this molybdate is in the middle part of the $AgRE(MoO_4)_2$ order and provides a possibility for a wide-range substitution of the Gd^{3+} ion by other RE^{3+} ions.

The SEM images of AGM and AGM:xHo,yYb samples are shown in Figure 4 and Figure S1, respectively. It can be stated that the final products are characterized by a homogeneous morphology. There are no specific morphological features that could be attributed to doping effects. The particle partial coalescence into agglomerates is observed in all samples. The particle size range is around 3–5 μm. Such a morphology is assumed to be induced by the material inter-diffusion between the heated grains at 600–850 °C.

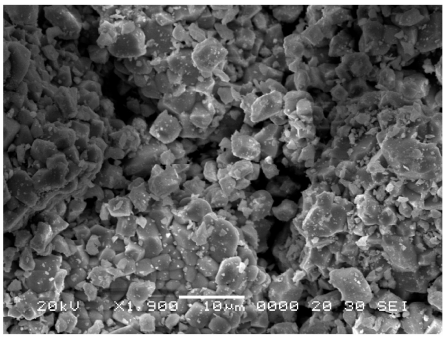

Figure 4. Scanning electron microscopy image of the synthesized $AgGd(MoO_4)_2$ sample.

In Figure 5, the UC emission spectra of AGM:0.05Ho,yYb samples are shown, and the intensity of UC luminescence is presented in the logarithmic scale. The known schematic energy level diagrams of Ho^{3+} (activator) and Yb^{3+} (sensitizer) ions in the AGM:0.05Ho,yYb samples and the UC mechanisms, accounting for the green and red emissions under the 980 nm laser excitation, are given in Figure 6. Under the excitation at 980 nm, the doped samples AGM:0.05Ho,yYb exhibited a yellowish green emission composed of red and green emission bands. At the red and green wavelengths, the Ho^{3+} ions show strong transitions $^5F_5 \rightarrow {}^5I_8$ and $^5S_2/^5F_4 \rightarrow {}^5I_8$, respectively. In the UC intensity competition between the samples, the AGM:0.05Ho,0.45Yb particles provide the strongest 545 and 655 nm emission bands. Other samples in emission intensity are in the order of AGM:0.05Ho,0.35Yb, AGM:0.05Ho,0.40Yb, and AGM:0.05Ho,0.50Yb. Thus, the optimal Yb^{3+}/Ho^{3+} ratio is revealed to be 9:1. The UC luminescence intensity at the main bands drastically increases as the Yb content grows from 0.35 to 0.4, then continues to increase at a slower rate as x grows from 0.4 to 0.45, and then drops as x grows to 0.5. This means that, at x approximately equal to 0.3, the critical distance condition for the energy transfer is achieved between the Ho^{3+} ion and a pair of simultaneously excited Yb^{3+} ions in the vicinity of the same Ho^{3+} ion. At x > 0.45, the number of simultaneously excited Yb^{3+} ions at the range within the critical distance of the energy transfer exceeds 2, and the excitation of extra Yb^{3+} ion cannot contribute to the two-step UC process; therefore, an additional excited Yb^{3+} ion is unable to transfer its energy to Ho^{3+} and decays back to the ground state. One should mention that the UC luminescence intensity distribution between red and green channels in AGM:0.05Ho,yYb is featured by the domination of the red channel, like in most of the earlier studied molybdate [10,56,57] and tungstate hosts, except for $NaPbLa(WO_4)_3$ [34]. Therefore, the unique effect of Pb on the crystalline lattice in $NaPbLa(WO_4)_3$ is not reproduced in the case of $AgGd(MoO_4)_2$.

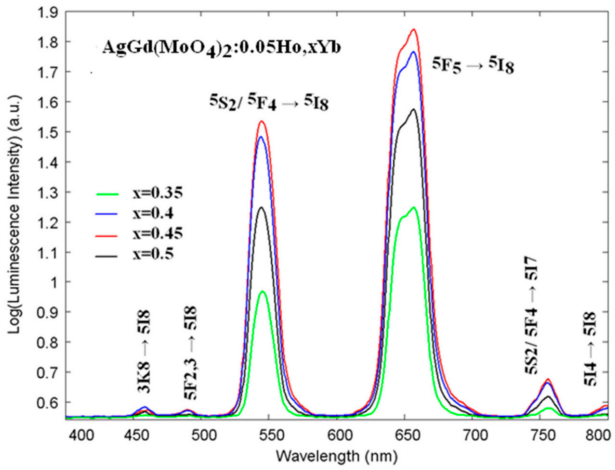

Figure 5. The upconversion (UC) output emission spectra of (**a**) $AgGd_{0.6}Ho_{0.05}Yb_{0.35}(MoO_4)_2$, (**b**) $AgGd_{0.55}Ho_{0.05}Yb_{0.40}(MoO_4)_2$, (**c**) $AgGd_{0.50}Ho_{0.05}Yb_{0.45}(MoO_4)_2$, and (**d**) $AgGd_{0.45}Ho_{0.05}Yb_{0.50}(MoO_4)_2$ excited by 980 nm at room temperature.

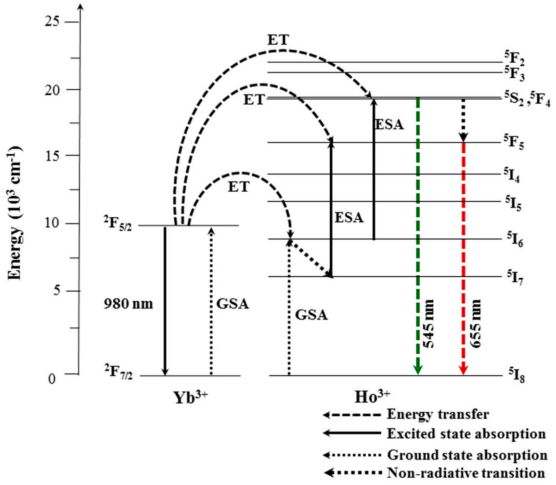

Figure 6. The schematic energy level diagrams of Yb^{3+} (sensitizer) and Ho^{3+} (activator) ions in the $AgGd_{0.95-y}Ho_{0.05}Yb_y(MoO_4)_2$ system and the upconversion mechanisms of the green and red emissions under 980 nm laser excitation: ET (energy transfer), ESA (Excited state absorption), GSA (Ground state absorption).

Besides two main UC luminescence bands specified above, several minor luminescent bands are observable in a logarithmic spectrum. First of all, the weakest band peaking at 490 nm should be mentioned. This peak should be ascribed to the $^5F_{2,3} \rightarrow {}^5I_8$ transition that starts from two closely lying states that have the smallest detuning for the two-photon cooperative UC process under the 980 nm pumping. Therefore, these states are expected to be primarily populated via the UC process and, in the absence of relaxation, the band at 490 nm would be the highest one. The extreme weakness of this band indicates the efficient relaxation of the population of initially excited levels that can happen via two possible channels, namely, via the decay to $^5S_2/^5F_4$ and via the cross-relaxation to $^5F_5$. Relative suppression of the cross-relaxation in the $NaPbLa(WO_4)_3$ lattice can be the origin of equalization of the red and green bands discovered earlier [34]. As we see, in AGM, the intensity of both relaxation channels specified above is just the same as in the majority of other molybdate and tungstate hosts, where Ho^{3+} upconversion was studied earlier [10,56,57].

Another minor peak in the UC luminescence spectra is observed at 459 nm and should be ascribed to the $^3K_8 \rightarrow {}^5I_8$ transition. The starting level of this transition is too high to be populated directly by the

two-step process or thermal excitation from $^5F_{2,3}$. Therefore, the existence of the corresponding band admits the presence of some additional three-step UC process, most likely, cascading $^5S_2/^5F_4 \rightarrow {}^5G_3$ excitation via the energy transfer from the Yb^{3+} ion. The peak at 750 nm is assigned to the transition from the highly populated $^5S_2/^5F_4$ level to the excited $^5I_8$ state, and its weakness suggests that the branching ratio for this transition is not enhanced in the AGM host, with respect to other ones. However, the last observed peak at 800 nm is not frequently observed, and it can be tentatively assigned to the transition from the $^5I_4$ level populated from the closely lying $^5F_5$ state.

In Figure 7, the calculated chromaticity coordinates (x, y) and CIE chromaticity diagram are shown for the compositions of UC output emission spectra of (a) $AgGd_{0.6}Ho_{0.05}Yb_{0.35}(MoO_4)_2$, (b) $AgGd_{0.55}Ho_{0.05}Yb_{0.40}(MoO_4)_2$, (c) $AgGd_{0.50}Ho_{0.05}Yb_{0.45}(MoO_4)_2$, and (d) $AgGd_{0.45}Ho_{0.05}Yb_{0.50}(MoO_4)_2$. The triangle depicted in Figure 7B indicates the standard coordinates for blue, green, and red colors. The inset in Figure 7B shows the chromaticity points for the samples (a), (b), (c), and (d). The chromaticity coordinates (x, y) are strongly dependent on the Ho^{3+}/Yb^{3+} concentration ratio. As shown in Figure 7A, the calculated chromaticity coordinates x = 0.388 and y = 0.394 for (a) $AgGd_{0.6}(MoO_4)_2$:$Ho_{0.05}Yb_{0.35}$, x = 0.407 and y = 0.432 for (b) $AgGd_{0.55}(MoO_4)_2$:$Ho_{0.05}Yb_{0.40}$, x = 0.399 and y = 0.424 for (c) $AgGd_{0.50}(MoO_4)_2$:$Ho_{0.05}Yb_{0.45}$, and x = 0.363 and y = 0.364 for (d) $AgGd_{0.45}(MoO_4)_2$:$Ho_{0.05}Yb_{0.5}$ correspond to the standard equal energy point in the CIE diagram shown in Figure 7B.

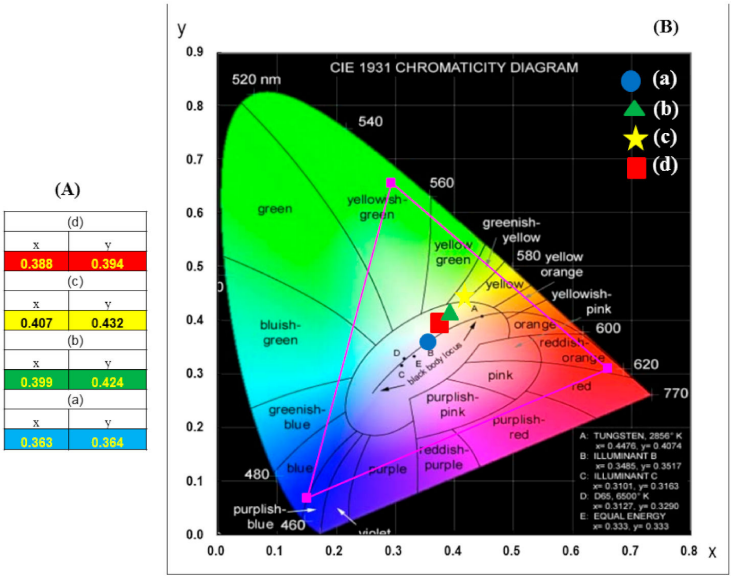

Figure 7. (**A**) Calculated chromaticity coordinates (x, y) values and (**B**) CIE chromaticity diagram for $AgGd(MoO_4)_2$:Ho^{3+}/Yb^{3+}phosphors. In the inset are the emission points for the synthesized (a) $AgGd_0(MoO_4)_2$, (b) $AgGd_{0.6}Ho_{0.05}Yb_{0.35}(MoO4)_2$, (c) $AgGd_{0.55}Ho_{0.05}Yb_{0.40}(MoO_4)_2$, (d) $AgGd_{0.50}Ho_{0.05}Yb_{0.45}(MoO_4)_2$, and (e) $AgGd_{0.45}Ho_{0.05}Yb_{0.50}(MoO_4)_2$ samples.

The Raman spectra of AGM:*x*Ho,*y*Yb (*x* = 0, 0.05; *y* = 0, 0.35, 0.4, 0.45, 0.5) powder samples are presented in Figure 8. As shown above, all compounds under consideration have the tetragonal ST-type structure (space group $I4_1/a$, $C_{4h}{}^6$ symmetry) and they consist of MoO_4 tetrahedra and $(Ag/Gd/Ho/Yb)O_8$ polyhedra. The high-frequency boundary of spectral bands related to the vibrations of AGM structural units is expressed by a high-intensity peak of the ν_1 MoO_4 symmetric stretching vibration typical of ST molybdates [10,22,24,58]. In case of the samples doped with Ho^{3+}/Yb^{3+} ions, the extra spectral bands associated with the luminescence of Ho^{3+} ions appear in the high wavenumber part of the spectra, as seen in Figure 8. The medium intensity spectral bands in the range of 730–835 cm^{-1} are attributed to the ν_3 asymmetric stretching vibrations of $[MoO_4]^{2-}$ ions. The internal stretching and bending vibrations of molybdate tetrahedra are separated by the gap over 430–730 cm^{-1} [9]. The ν_4 MoO_4 bending modes appear in the range of 365–435 cm^{-1}. The ν_2 bending vibrations can be observed

in Figure 8 as the strong bands in the range from 290 to 350 cm^{-1}. The Raman band at 201 cm^{-1} is identified as a free rotation of molybdate tetrahedra [24]. The remaining modes below 200 cm^{-1} are attributed to the translations of MoO_4 and vibrations of (Ag/Gd/Ho/Yb)O_8 polyhedra.

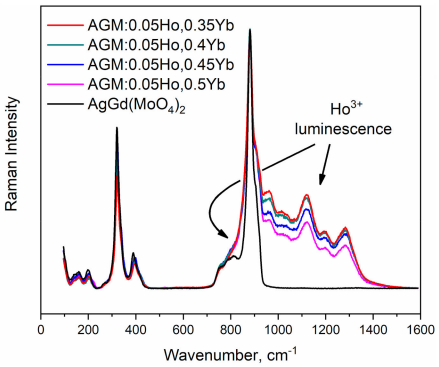

Figure 8. Raman spectra of AGM and AGM:xHo,yYb (x = 0.05; y = 0.35, 0.4, 0.45, 0.5) samples.

It can be seen from the group theory calculations that the primitive cell of AGM has 30 vibration modes, and the mechanical representation in the center of Brillouin zone can be written as follows: $\Gamma_{vibr} = 3A_g + 6B_g + 6E_g + 6A_u + 3B_u + 6E_u$, where g-labeled modes are active in the Raman spectrum, A_u and E_u—modes are active in the infrared spectrum, and B_u modes are silent. In Table 5, one can check the number of active spectral bands in Raman and infrared spectra related to the internal vibrations of $[MoO_4]^{2-}$ ions [58]. The ST oxides with the C_{4h} symmetry should show only one spectral band related to the ν_1 MoO_4 symmetric stretching vibration, but an extra band appears as the right shoulder of the high-intensity peak at 880 cm^{-1} (Figure 8). Such spectral characteristic can be due to the fact that the crystal can have symmetry lower than C_{4h}, for example, S_4 (I–4 space group) [11]. In this case, the crystal structure contains two crystallographically independent MoO_4 tetrahedra and the Raman spectra should be more in line in the range of their vibrations. On the other hand, the local distortions of $[MoO_4]^{2-}$ ions in the structure may occur because of the fact that the occupancy of Ag and Gd atoms in AGM is not equal to one (Table 2), and even a small difference in Mo-O bond lengths can cause the displacements of symmetric stretching vibration wavenumber. As mentioned above, B_u modes are silent in ST crystals. However, in the case of some $AgRE(MoO_4)_2$ (RE = La-Nd and Sm) [54], they become infrared active and appear, for example, as the $[MoO_4]^{2-}$ ion symmetric stretching vibration that is in agreement with Table 5. At the same time, the appearance of such a spectral band in the infrared spectrum cannot be described in the framework of the structure with the S_4 symmetry, because the vibration mode labeled as A (Table 5) should be active only in the Raman spectrum.

Table 5. Correlation diagram for the MoO_4 tetrahedra in structures with C_{4h} and S_4 symmetry.

Free Ion T_d	**Site** S_4	**Factor Group** C_{4h}
ν_1, (A_1)	A	$A_g + B_u$
ν_2, (A_1)	A+B	$A_g + B_u + A_u + B_g$
ν_3, ν_4 (T_2)	B+E	$A_u + B_g + E_g + E_u$
Free ion T_d	**Site** S_4	**Factor Group** S_4
ν_1, (A_1)	A	A
ν_2, (A_1)	$A + B$	$A + B$
ν_3, ν_4 (T_2)	$B + E$	$B + E$

4. Conclusions

The $AgGd_{1-x}(MoO_4)_2$:Ho^{3+}/Yb^{3+} double molybdates with five Ho^{3+}/Yb^{3+}doping levels were synthesized by the MES-based process, and the refinement of their crystal structure was implemented for the first time. The effects of solid solution composition and spectroscopic characteristics were investigated. The phosphor samples heated at 850 °C for 16 h showed the fine and homogeneous morphology with particles sized 3–5 μm. The powder diffraction data of $AgGd(MoO_4)_2$:*x*Ho,*y*Yb ($x = 0, 0.05$; $y = 0, 0.35, 0.4, 0.45, 0.5$) for Rietveld analysis were collected at room temperature and the crystal structures were determined in the tetragonal space group $I4_1/a$ with parameters close to those of $AgEu(MoO_4)_2$ and $NaGd(MoO_4)_2$. The site of (Ag/Eu) or (Na/Gd) ion was occupied by Ag^+, Gd^{3+}, Ho^{3+}, and Yb^{3+} ions with fixed occupations, and led to low R-factors. The linear decrease of the cell volume was observed on the doping level increase. In the UC measurements, using the excitation at 980 nm, the resultant phosphors showed yellowish green output emissions derived from the strong $^5S_2/^5F_4 \rightarrow {}^5I_8$ and $^5F_5 \rightarrow {}^5I_8$ transitions of Ho^{3+} ions. The optimal concentration ratio Yb^{3+}:Ho^{3+} was revealed to be 9:1. The behavior of UC intensity is dependent on the Yb/Ho ratio and is explained in terms of the optimal number of Yb^{3+} ions at the characteristic energy transfer distance around the Ho^{3+} ion. The room temperature Raman spectra were analyzed to obtain information on the AGM:xHoyYb crystal structure. The nature of extra bands was explained in the framework of the local distortions of MoO_4 tetrahedra.

Supplementary Materials: The following are available online at http://www.mdpi.com/2073-4352/10/11/1000/s1.

Author Contributions: Conceptualization, A.A.; Data curation, C.S.L.; Investigation, C.S.L., A.A., V.A., M.M. and A.O. All authors have read and agreed to the published version of the manuscript.

Funding: This study was supported by the Research Program through the Campus Research Foundation funded by Hanseo University in 2020 (201Yunghap09).

Conflicts of Interest: The authors declare no conflict of interest.

References

1. Wang, M.; Abbineni, G.; Clevenger, A.; Xu, S. Upconversion nanoparticles: Synthesis, surface modification and biological applications. *Nanomed. Nanotech. Biol. Med.* **2011**, *7*, 710–729. [CrossRef] [PubMed]
2. Lin, M.; Zhao, Y.; Wang, S.; Liu, M.; Duan, Z.; Chen, Y.; Li, F.; Xu, F.; Lu, T.J. Recent advances in synthesis and surface modification of lanthanide-doped upconversion nanoparticles for biomedical applications. *Biotechnol. Adv.* **2012**, *30*, 1551–1561. [CrossRef] [PubMed]
3. DaCosta, M.V.; Doughan, S.; Han, Y.; Krull, U.J. Lanthanide upconversion nanoparticles and applications in bioassays and bioimaging: A review. *Anal. Chim. Acta* **2014**, *832*, 1–33. [CrossRef] [PubMed]
4. Zhou, J.; Liu, Q.; Feng, W.; Sun, Y.; Li, F. Upconversion luminescent materials: Advances and applications. *Chem. Rev.* **2015**, *115*, 395–465. [CrossRef]
5. Atuchin, V.V.; Chimitova, O.D.; Gavrilova, T.A.; Molokeev, M.S.; Kim, S.J.; Surovtsev, N.V.; Bazarov, B.G. Synthesis, structural and vibrational properties of microcrystalline $RbNd(MoO_4)_2$. *J. Cryst. Growth* **2011**, *318*, 683–686. [CrossRef]
6. Morozov, V.A.; Bertha, A.; Meert, K.W.; Van Rompaey, S.; Batuk, D.; Martinez, G.T.; Van Aert, S.; Smet, P.F.; Raskina, M.V.; Poelman, D.; et al. Incommesurate modulation and luminescence in the $CaGd_{2(1-x)}Eu_{2x}(MoO_4)_{4(1-y)}(WO_4)_{4y}$ ($0 \le x \le 1$, $0 \le y \le 1$) red phosphors. *Chem. Mater.* **2013**, *25*, 4387–4395. [CrossRef]
7. Lim, C.S. Upconversion photoluminescence properties of $SrY_2(MoO_4)_4$:Er^{3+}/Yb^{3+} phosphors synthesized by a cyclic microwave-modified sol-gel method. *Inf. Phys. Technol.* **2014**, *67*, 371–376. [CrossRef]
8. Shi, P.; Xia, Z.; Molokeev, M.S.; Atuchin, V.V. Crystal chemistry and luminescence properties of red-emittig $CsGd_{1-x}Eu_x(MoO_4)_2$ solid-solution phosphors. *Dalton Trans.* **2014**, *43*, 9669–9676. [CrossRef]
9. Atuchin, V.V.; Aleksandrovsky, A.S.; Chimitova, O.D.; Gavrilova, T.A.; Krylov, A.S.; Molokeev, M.S.; Oreshonkov, A.S.; Bazarov, B.G.; Bazarova, J.G. Synthesis and spectroscopic properties of monoclinic α-$Eu_2(MoO_4)_2$. *J. Phys. Chem. C* **2014**, *118*, 15404–15411. [CrossRef]

10. Lim, C.S.; Aleksandrovsky, A.; Molokeev, M.; Oreshonkov, A.; Atuchin, V. The modulated structure and frequency upconversion properties of $CaLa_2(MoO_4)_4$:Ho^{3+}/Yb^{3+} phosphors prepared by microwave synthesis. *Phys. Chem. Chem. Phys.* **2015**, *17*, 19278–19287. [CrossRef] [PubMed]
11. Cheng, F.; Xia, Z.; Jing, X.; Wang, Z. Li/Ag ratio dependent structure and upconversion photoluminescence of $Li_xAg_{1-x}Yb_{0.99}(MoO_4)_2$:$0.01Er^{3+}$ phosphors. *Phys. Chem. Chem. Phys.* **2015**, *17*, 3689–3696. [CrossRef]
12. Lim, C.S. Highly modulated structure and upconversion photoluminescence properties of $PbGd_2(MoO_4)_4$:Er^{3+}/Yb^{3+} phosphors. *Mater. Res. Bull.* **2016**, *75*, 211–216. [CrossRef]
13. Yakovlev, V.G.; Mikhailin, V.V.; Romanenko, A.Y.; Basovich, O.M.; Khaikina, E.G. Spectral-luminescent properties of $AgLa_{1-x}Eu_x(MoO_4)_2$ solid solutions. *Mosc. Univ. Phys. Bull.* **2009**, *64*, 519–522. [CrossRef]
14. Benoît, G.; Véronique, J.; Arnaud, A.; Alain, G. Luminescence properties of tungstates and molybdates phosphors: Illustration on $ALn(MO_4)_2$ compounds (A = alikaline cation, Ln = lanthanides, M = W, Mo). *Solid State Sci.* **2011**, *13*, 460–467. [CrossRef]
15. Li, T.; Guo, C.; Wu, Y.; Li, L.; Jeong, J.H. Green upconversion luminescence in Yb^{3+}/Er^{3+} co-doped $ALn(MoO_4)_2$ (A = Li, Na and K.; Ln = La, Gd and Y). *J. Alloys Compd.* **2012**, *540*, 107–112. [CrossRef]
16. Hou, L.; Cui, S.; Fu, Z.; Wu, Z.; Fu, X.; Jeong, J.H. Facile template free synthesis of $KLa(MoO_4)_2$: Eu^{3+},Tb^{3+} microspheres and their multicolor tunable luminescence. *Dalton Trans.* **2014**, *43*, 5382–5392. [CrossRef] [PubMed]
17. Wang, Q.F.; Liu, Y.; Wang, Y.; Wang, W.; Wan, Y.; Wang, G.G.; Lu, Z.G. Considerable photoluminescence enhancement of $LiEu(MoO_4)_2$ red phosphors via Bi and/or Si doping for white LEDs. *J. Alloys Compd.* **2015**, *625*, 355–361. [CrossRef]
18. Li, T.; Guo, C.; Zhou, S.; Duan, C.; Yin, M. Highly sensitive optical thermometry of Yb^{3+}-Er^{3+}codoped$AgLa(MoO_4)_2$ green upconversion phosphor. *J. Am. Ceram. Soc.* **2015**, *98*, 2812–2816. [CrossRef]
19. Li, X.; Lin, Z.; Zhang, L.; Wang, G. Growth, thermal and spectral properties of Nd^{3+}-doped $NaGd(MoO_4)_2$ crystal. *J. Cryst. Growth* **2006**, *290*, 670–673. [CrossRef]
20. Zhou, W.W.; Wei, B.; Zhao, W.; Wang, G.F.; Bao, X.; Chen, Y.H.; Wang, F.W.; Du, J.-M.; Yu, H.-J. Intense yellow emission in Dy^{3+}-doped $LiGd(MoO_4)_2$ crystal for visible lasers. *Opt. Mater.* **2011**, *34*, 56–60. [CrossRef]
21. Yu, Y.; Zhang, L.; Huang, Y.; Lin, Z.; Wang, G. Growth, crystal structure, spectral properties and laser performance of Yb^{3+}:$NaLu(MoO_4)_2$ crystal. *Laser Phys.* **2013**, *23*, 105807. [CrossRef]
22. Lim, C.S.; Aleksandrovsky, A.S.; Molokeev, M.S.; Oreshonkov, A.S.; Atuchin, V.V. Microwave synthesis and spectroscopic properties of ternary scheelite-type molybdate phosphors $NaSrLa(MoO_4)_2$:Er^{3+},Yb^{3+}. *J. Alloys Compd.* **2017**, *713*, 156–163. [CrossRef]
23. Subbotin, K.A.; Titov, A.I.; Lis, D.A.; Sani, E.; Smirnov, V.A.; Alimov, O.K.; Zharikov, E.V.; Shcherbakov, I.A. Donor centers involved into the quantum cutting in ytterbium-doped scheelite-like crystals. *Phys. Stat. Sol. A* **2020**, *217*, 1900659. [CrossRef]
24. Lim, C.S.; Aleksandrovsky, A.S.; Atuchin, V.V.; Molokeev, M.S.; Oreshonkov, A.S. Microwave so-gel synthesis, microstructural and spectroscopic properties of scheelite-type ternary molybdate upconversion phosphor $NaPbLa(MoO_4)_2$:Er^{3+},Yb^{3+}. *J. Alloys Compd.* **2020**, *826*, 152095. [CrossRef]
25. Kroutko, V.; Belik, A.; Lysanova, G.; Komova, M. *ICDD Grant-In-Aid (2001), PDF Number: 53–42*; Institute of General and Inorganic Chemistry RAS: Moscow, Russia, 2001.
26. Wang, W.; Liu, N.; Du, Y.; Wang, Y.; Li, L.; Jiao, H. Up-conversion luminescence properties of Yb^{3+}/Er^{3+} co-doped $AgGd(W,Mo)_2O_8$ phosphors. *J. Alloys Compd.* **2013**, *577*, 426–430. [CrossRef]
27. Song, J.; Du, Y.; Xu, L.; Wei, H.; He, D.; Jiao, H. Synthesis of red-emitting $AgGd_{0.9}Eu_{0.1}(MoO_4)_2$ phosphors by precipitation at room temperature. *J. Am. Ceram. Soc.* **2014**, *97*, 1442–1449. [CrossRef]
28. Auzel, F. Upconversion and anti-Stokes processes with f and d ions in solids. *Chem. Rev.* **2004**, *104*, 139–173. [CrossRef] [PubMed]
29. Rybakov, K.I.; Olevsky, E.A.; Krikun, E.V. Microwave sintering: Fundamentals and modeling. *J. Am. Ceram. Soc.* **2013**, *96*, 1003–1020. [CrossRef]
30. Kitchen, H.J.; Vallance, S.R.; Kennedy, J.L.; Tapia-Ruiz, N.; Carassiti, L.; Harrison, A.; Whittaker, A.G.; Drysdale, T.D.; Kingman, S.W.; Gregory, D.H. Modern microwave methods in solid-state inorganic materials chemistry: From fundamentals to manufacturing. *Chem. Rev.* **2014**, *114*, 1170–1206. [CrossRef]
31. Lim, C.S. Cyclic MAM synthesis and upconversion photoluminescence properties of $CaMoO_4$:Er^{3+}/Yb^{3+} particles. *Mater. Res. Bull.* **2012**, *47*, 4220–4225. [CrossRef]

32. Lim, C.S. Synthesis of $SrMoO_4:Er^{3+}/Yb^{3+}$ particles by a cyclic MAM method and their upconversion photoluminescence properties. *Mater. Res. Bull.* **2013**, *48*, 3805–3810. [CrossRef]
33. Lim, C.S.; Aleksandrovsky, A.; Molokeev, M.; Oreshonkov, A.; Atuchin, V. (Microwave sol-gel synthesis and upconversion photoluminescence properties of $CaGd_2(WO_4)_4:Er^{3+}/Yb^{3+}$ phosphors with incommensurately modulated structure. *J. Solid State Chem.* **2015**, *228*, 160–166. [CrossRef]
34. Lim, C.S.; Atuchin, V.V.; Aleksandrovsky, A.S.; Denisenko, Y.G.; Molokeev, M.S.; Oreshonkov, A.S. Fabrication of microcrystalline $NaPbLa(WO_4)_3:Yb^{3+}/Ho^{3+}$ phosphors and their upconversion photoluminescent characteristics. *Korean J. Mater. Res.* **2019**, *29*, 741–746. [CrossRef]
35. Bruker AXS. *TOPAS V4: General Profile and Structure Analysis Software for Powder Diffraction Data.—User's Manual*; Bruker AXS: Karlsruhe, Germany, 2008.
36. Cheng, F.; Xia, Z.; Molokeev, M.S.; Jing, X. Effects of composition modulation on the luminescence properties of Eu^{3+} doped $Li_{1-x}Ag_xLu(MoO_4)_2$ solid-solution phosphors. *Dalton Trans.* **2015**, *44*, 18078–18089. [CrossRef]
37. McIlvried, M. *ICDD Grant-In-Aid*; Penn State University: University Park, PA, USA, 1973; pp. 25–828.
38. Klevtsov, P.V.; Kozeeva, L.P. Synthesis of binary lithium molybdates containing rare earth elements and Y, Izv. *Akad. Nauk SSSR. Neorg. Mater.* **1969**, *5*, 1842–1843. (In Russian)
39. Kolitsch, U. The crystal structures of phenacite-type $Li_2(MoO_4)$, and scheelite-type $LiY(MoO_4)_2$ and $LiNd(MoO_4)_2$. Z. *Kristallog* **2001**, *216*, 449–454. [CrossRef]
40. Savel'eva, M.V.; Shakhno, I.V.; Plyuschev, V.E.; Kotlyar, A.A. Investigation of interaction of molybdates sodium with molybdates of dysprosium, holmium, erbium. *Izv. VUZ. Zvetnaya Metall.* **1969**, *2*, 85–89.
41. Mokhosoev, M.V.; Kockot, I.F.; Kononenko, I.S. Study of double molybdates of lanthanum and alkali metal with molybdates of alkali metals in melting. *Russ. J. Inorg. Chem. (Engl. Transl.)* **1970**, *5*, 271–274.
42. Egorova, A.N.; Majer, A.A.; Nevskij, N.N.; Provotvorov, M.V. The crystal structure of $LiCe(MoO_4)_2$. *Izv. Akad. Nauk Sssr Neorg. Mater.* **1982**, *18*, 2036–2038.
43. Perera, S.S.; Rabuffetti, F.A. NIR-to-NIR and NIR-to-blue light upconversion in stoichiometric $NaYb(MO_4)_2$ (M = Mo, W). *Cryst. Eng. Comm.* **2016**, *18*, 5818–5825. [CrossRef]
44. Zhao, D.; Li, F.; Cheng, W.; Zhang, H. Scheelite-type $NaEr(MoO_4)_2$. *Acta Cryst.* **2010**, *66*, i36. [CrossRef]
45. Stedman, N.J.; Cheetham, A.K.; Battle, P.D. Crystal structures of two sodium yttrium molybdates: $NaY(MoO_4)_2$ and $Na_5Y(MoO_4)_4$. *J. Mater. Chem.* **1994**, *4*, 707–711. [CrossRef]
46. Cortese, A.J.; Abeysinghe, D.; Smith, M.D.; zur Loye, H.C. Single crystal growth and characterization of $Na_xLn_{1-x}MoO_4$, Ln=La, Ce, Pr, Nd, Sm, and Eu (x = 0.397–0.499). *J. Solid State Chem.* **2016**, *240*, 76–81. [CrossRef]
47. Schleid, T.; Hartenbach, I. Scheelite-type sodium neodymium (III) ortho-oxidomolybdate (VI), $NaNd[MoO_4]_2$. *Acta Cryst. E* **2011**, *67*, i71. [CrossRef]
48. Teller, R.G. Refinement of some $Na_{0.5-x}M'_{0.5+x/3}\square_{2x/3}MoO_4$, M = Bi, Ce, La, scheelite structures with powder neutron and X-ray diffraction data. *Acta Cryst. C* **1992**, *48*, 2101–2104. [CrossRef]
49. Stevens, S.B.; Morrison, C.A.; Allik, T.H.; Rheingold, A.L.; Haggerty, B.S. $NaLa(MoO_4)_2$ as a laser host material. *Phys. Rev. B* **1991**, *43*, 7386–7394. [CrossRef]
50. Wanklyn, B.M.; Wondre, F.R. Flux growth of crystals of $RKMo_2O_8$, R_2MoO_6 and R_6MoO_{12} in the systems R_2O_3-K_2O-MoO_3. *J. Cryst. Growth* **1978**, *43*, 93–100. [CrossRef]
51. Klevtsov, P.V.; Kozeeva, L.P.; Pavlyuk, A.A. Polymorphism and crystallization of potassium-rare earth molybdates, $KLn(MoO_4)_2$ (Ln = La, Ce, Pr, Nd). *Kristallografiya* **1975**, *20*, 1216–1220.
52. Kroutko, V.; Lysanova, G.; Komova, M. *ICDD Grant-In-Aid 2003; PDF Number: 54-1222; PDF Number 54-1223; PDF Number: 54-1220*; Institute of General and Inorganic Chemistry, RAS: Moscow, Russia, 2003.
53. Kroutko, V.; Lysanova, G.; Komova, M. *ICDD Grant-In-Aid 2002; PDF Number: 54-901*; Institute of General and Inorganic Chemistry, RAS: Moscow, Russia, 2002.
54. Shi, F.; Meng, J.; Ren, Y. Preparation structure and physical properties of new silver lanthanide molybdenum oxides [$AgLnMo_2O_8$ (Ln = La-Nd and Sm)]. *Mater. Res. Bull.* **1995**, *30*, 1401–1405. [CrossRef]
55. Bushuev, N.N.; Trunov, V.K.; Gizhinsky, A.R. X-ray diffraction study of rare earth molybdates with the structure of $KSm(MoO_4)_2$. *Russ. J. Inorg. Chem.* **1973**, *18*, 2865–2866. (In Russian)
56. Lim, C.S.; Atuchin, V.V.; Aleksandrovsky, A.S.; Molokeev, M.S.; Oreshonkov, A.S. Incommensurately modulated structure and spectroscopic properties of $CaGd_2(MoO_4)_4:Ho^{3+}/Yb^{3+}$ phosphors for up-conversion applications. *J. Alloys Compd.* **2017**, *695*, 737–746. [CrossRef]

57. Lim, C.S.; Aleksandrovsky, A.S.; Molokeev, M.S.; Oreshonkov, A.S.; Ikonnikov, D.A.; Atuchin, V.V. Triple molybdatescheelite-type unconversion phosphor $NaCaLa(MoO_4)_3:Er^{3+}/Yb^{3+}$: Structural and spectroscopic properties. *Dalton Trans.* **2016**, *45*, 15541–15551. [CrossRef] [PubMed]
58. Kroumova, E.; Aroyo, M.I.; Perez-Mato, J.M.; Kirov, A.; Capillas, C.; Ivantchev, S.; Wondratschek, H. Bilbao crystallographic server: Useful databases and tools for phase-transition studies. *Phase Transit.* **2003**, *76*, 155–170. [CrossRef]